NASA Technical Memorandum 105625

Flutter Analysis of a Supersonic Cascade in Time Domain Using an ADI Euler Solver

T.S.R. Reddy and M.A. Bakhle
University of Toledo
Toledo, Ohio

and

D.L. Huff
Lewis Research Center
Cleveland, Ohio

April 1992

NASA

FLUTTER ANALYSIS OF A SUPERSONIC CASCADE IN TIME DOMAIN USING AN ADI EULER SOLVER

T.S.R. Reddy* and Milind A. Bakhle*
University of Toledo
Toledo, Ohio 43606

and

Dennis L. Huff
National Aeronautics and Space Administration
Lewis Research Center
Cleveland, Ohio 44135

E-6966

SUMMARY

The aeroelastic stability of a two-dimensional cascade oscillating in supersonic axial flow is analyzed in the time domain. the aeroelastic model consists of a single-degree-of-freedom typical section structural model for each blade of the cascade and an unsteady two-dimensional cascade aerodynamic model based on the Euler equations. The Euler equations are solved using a time-accurate Alternating Direction Implicit (ADI) solution scheme. The aeroelastic equations are integrated in time. The effect of interblade phase angle is included in the aeroelastic analysis by an appropriate choice of initial and boundary conditions.

Flutter predictions are obtained from the time response of a flat plate cascade in single-degree-of-freedom pitching motion. The results correlate well with those obtained from a separate frequency domain flutter analysis for all values of interblade phase angles considered. Flutter results are then presented for cascades having airfoil sections representative of a supersonic throughflow fan. The validity of the time integration method for a cascade of airfoils at various interblade phase angles is demonstrated.

NOMENCLATURE

a	speed of sound
b	airfoil semichord
C_α	damping coefficient in pitching
C_p	steady pressure coefficient $= 2(p - p_1)/\rho_1 V_1^2$
c	airfoil chord
c_m	moment coefficient about elastic axis
e	total energy of the fluid per unit volume
F,G	fluxes of mass, momentum, and energy in x,y direction
g/c	gap-to-chord ratio
$\mathrm{Im}\{c_m\}$	imaginary component of c_m

*NASA Resident Research Associate at Lewis Research Center.

I_α	mass moment of inertia about elastic axis
i	incidence angle
J	Jacobian of transformation
K_α	spring constant for pitching
k_b	reduced frequency based on semichord
M	Mach number
m	mass per unit length
N	number of blades in the cascade
Q_α	generalized force in pitching
q	vector of flow variables in x,y coordinates
r_α	radius of gyration about elastic axis
t	time
t/c	thickness-to-chord ratio
u,v	x,y velocity components normalized by the speed of sound
V	total velocity
V^*	nondimensional speed, $V^* = V_1/b\omega_\alpha$
x,y	Cartesian coordinate system
x′	distance measured from leading edge to trailing edge
α	pitching (torsion) displacement, positive nose up, see figure 1(b)
α_0	steady component of pitching displacement α
α_1	unsteady component of pitching displacement α
β	inlet flow angle
γ	ratio of specific heats
θ	stagger angle
μ	mass ratio
ξ	chordwise direction of transformed coordinate system
η	normal direction of transformed coordinate system
ζ_α	critical damping factor in pitching
ρ	air density
σ	interblade phase angle
τ	nondimensional time
ω	frequency of forced oscillation
ω_α	pitching frequency, $\omega_\alpha = (K_\alpha/I_\alpha)^{1/2}$

Subscripts and superscripts:

$(\dot{})$	$d( )/dt$
$(\ddot{})$	$d^2( )/dt^2$
$( )'$	$d( )/d\tau$
$( )''$	$d^2( )/d\tau^2$
F	evaluated at flutter
1	evaluated at inlet

INTRODUCTION

Recently there has been interest in designing a turbine engine that operates with supersonic flow through the rotor and stator blade rows of the fan. The supersonic throughflow (SSTF) fan is expected to provide about a 10-percent decrease in specific fuel consumption, and about a 25-percent reduction in propulsion weight, which would lead to a 22-percent increase in aircraft range (ref. 1). Other advantages of the SSTF include fewer fan stages for a given pressure ratio, less inlet cowl and boundary layer bleed drag, better inlet pressure recovery, and better matching of bypass ratio variation to flight speed. NASA Lewis Research Center has initiated an exploratory program to investigate the feasibility of the SSTF fan (refs. 1 to 4).

One of the aspects to be considered in the safe design of the SSTF fan is possible aeroelastic instability such as flutter. However, no experimental data is currently available and only numerical studies have been undertaken. Because of the complexity involved in modeling supersonic throughflow in a three-dimensional rotor or stator blade row, only two-dimensional analyses have been attempted in the literature.

In these two-dimensional analyses, the rotor or stator is modeled as a rectilinear two-dimensional cascade of airfoils with supersonic axial flow (refs. 5 to 8); this is also referred to as a two-dimensional cascade with a supersonic leading edge locus. Linearized equations (see, e.g., ref. 9) applicable for an unloaded, cascade of flat plate airfoils in inviscid flow have been used in these analyses. The motion of the airfoils in each mode of the cascade is assumed to be simple harmonic with a constant phase angle between the adjacent blades. This assumption leads to an eigenvalue problem in the frequency domain and the stability of the system is determined from the eigenvalues (ref. 10).

The above analyses have neglected the effects of airfoil thickness, camber, and steady-state angle of attack on supersonic cascade flutter. One way to include these effects in the cascade flutter analysis is by using Computational Fluid Dynamics (CFD) methods. Recent advances in the field of CFD with regard to the development of more efficient algorithms and increase in computer speeds and memory have made possible numerical studies aimed at computing the complex flow field associated with a supersonic axial flow cascade.

There is no published research on the aeroelastic analysis of a supersonic cascade with supersonic axial flow using the CFD approach. However, efforts to predict steady aerodynamic characteristics of supersonic compressor airfoils using Euler/Navier-Stokes equations have been reported in reference 11. Results from a two-dimensional, finite difference Euler cascade code for the analysis of unsteady supersonic axial flow have been reported in reference 12. The unsteady motion resulting from blade vibration is included in the analysis by using a deforming grid technique. This code has been validated by

comparing results for a flat plate airfoil with corresponding results from linear theory. The code is suitable for use in the aeroelastic analysis of SSTF fans.

The objective of the present investigation is to develop an aeroelastic analysis for the prediction of flutter in a cascade of airfoils by using a time integration method. The time integration method is necessary when aerodynamic and structural nonlinearities, such as shock motions, large amplitude oscillations, nonlinear elastic behavior, etc. are to be modeled. The classical frequency domain analysis is incapable of handling such nonlinearities. In addition, the time integration method has the following advantages. The response for both steady and unsteady loading can be obtained. The method gives a realistic simulation of the motions of both the fluid and the cascade. It may also allow a considerable saving in computational effort when analyzing cascade configurations with several degrees of freedom. Lastly, it allows the animation of motion of the cascade and the flow field for better understanding of the physical phenomenon.

The present study is restricted to a two-dimensional cascade model. A typical section representation of each of the blades of the cascade is assumed. Only a single-degree-of-freedom pitching motion is considered for the analysis. It is to be noted that the stability of a single-degree-of-freedom system, with no structural damping, can be assessed purely from the aerodynamic coefficients. However, the method being developed here will also be useful for systems with structural damping and with more than one degree of freedom. Note that this is the first instance that the time integration method is being applied to investigate aeroelastic stability of a cascade of airfoils.

The time integration method being used for flutter analysis consists of the simultaneous integration of the structural and fluid dynamics equations (ref. 13) of each blade in the cascade. The structural dynamics equations are written for each blade in the cascade, assuming that each blade is a typical section with pitching motion. The unsteady aerodynamic load terms that appear in the aeroelastic equations are calculated by using the unsteady two-dimensional, compressible, Euler cascade solver of reference 12. The loads determined by solving the fluid dynamic equations are used in the aeroelastic equations to determine the structural displacements. The displacements calculated from the aeroelastic equations are then used as input to the fluid dynamics equations to determine the loads. These two steps are repeated successively. In general, the displacements show an oscillatory variation with increasing time. If the amplitudes of the displacements grow in time, then flutter is said to occur.

A brief description of the method of analysis, the computational grids, and boundary conditions is given in the next section, followed by results and discussion. Time responses (variations of pitching amplitude with time) have been calculated for a flat plate cascade and a cascade of SSTF fan airfoils in supersonic axial flow. The flutter speeds calculated from the responses are compared with those obtained from a conventional frequency domain flutter analysis; the aerodynamic coefficients required for this frequency domain analysis are obtained by forcing the airfoils in harmonic motion.

At this time, there is no experimental data available to compare with the present calculations.

ANALYSIS

The rotor or stator is modeled as a two-dimensional rectilinear cascade of airfoils. Figure 1(a) shows the geometry and nomenclature for a tuned cascade; a tuned cascade is one in which all the blades have identical structural properties.

Aeroelastic Model

A typical section with only pitching motion is considered for each blade in the aeroelastic analysis. A typical section model of a blade is shown in figure 1(b). The typical section has pitching (α) displacement. The governing aeroelastic equation, which is applicable to each blade in the cascade, can be written as

$$I_\alpha \ddot{\alpha} + C_\alpha \dot{\alpha} + K_\alpha \alpha = Q_\alpha \tag{1}$$

where I_α is the mass moment of inertia about the elastic axis, C_α is structural damping parameter, K_α is the pitching spring constant, Q_α is the generalized force (moment about the pitching axis), and the dots over α denote differentiation with respect to time, t. Defining $r_\alpha^2 = I_\alpha/mb^2$, $\omega_\alpha^2 = K_\alpha/I_\alpha$, $\zeta_\alpha = C_\alpha/2\omega_\alpha I_\alpha$, where r_α is the radius of gyration, m is the mass, b is the semichord, ω_α is the natural pitching frequency, and ζ_α is the critical damping factor in pitching. Equation (1) can be written as

$$\left(\frac{r_\alpha}{2}\right)^2 \ddot{\alpha} + \left(\frac{\zeta_\alpha \omega_\alpha r_\alpha^2}{2}\right)\dot{\alpha} + \left(\frac{\omega_\alpha r_\alpha}{2}\right)^2 \alpha = \left(\frac{Q_\alpha}{4mb^2}\right) \tag{2}$$

The generalized force Q_α is related to the moment coefficient, c_m, about the pitching axis (elastic axis), as follows:

$$Q_\alpha = \frac{1}{2}\rho_1 V_1^2 (2b)^2 c_m \tag{3}$$

where V_1 and ρ_1 are the velocity and density evaluated at the inlet. Defining, nondimensional time and velocity as $\tau = ta_1/2b$ and $V^* = V_1/b\omega_\alpha$, where a_1 is the speed of sound at the inlet, and substituting equation (3) into equation (2), the final aeroelastic equations can be written as

$$\left(\frac{r_\alpha}{2}\right)^2 \alpha'' + \left(\frac{\zeta_\alpha r_\alpha^2 M}{V^*}\right)\alpha' + \left(\frac{r_\alpha M}{V^*}\right)^2 \alpha = \left(\frac{2c_m M^2}{\pi\mu}\right) \tag{4}$$

where $(\,)' = d(\,)/d\tau$, $M = V_1/a_1$, and $\mu = m/\pi\rho_1 b^2$.

The aeroelastic equation (eq. (4)) is marched in time using the constant average acceleration method (Newmark scheme) (ref. 14). It should be noted that at flutter, reduced frequency based on semichord, k_F, used in a frequency domain analysis (ref. 10) is related to flutter speed V_F^* and flutter frequency ω_F as

$$k_F = \frac{\omega_F b}{V_1} = \left(\frac{\omega_F/\omega_\alpha}{V_F^*}\right) \tag{5}$$

Aerodynamic Model

The moment coefficient (c_m) in equation (4), is calculated by integrating the pressure over the airfoil surface for each blade at each time step. The pressure distribution is obtained by solving the unsteady, two-dimensional, compressible Euler equations on a body-fitted coordinate system in strong conservation form using an alternating direction implicit (ADI) procedure. The present Euler code is based on the code developed for isolated airfoils in reference 15. A brief outline is given here. Further details of the formulation can be found in reference 12.

In the Cartesian coordinate system, the two-dimensional unsteady Euler equations may be written as

$$q_t + F_x + G_y = 0 \tag{6a}$$

where

$$q = \begin{pmatrix} \rho \\ \rho u \\ \rho v \\ e \end{pmatrix} \qquad F = \begin{pmatrix} \rho u \\ \rho u^2 + p \\ \rho uv \\ u(e + p) \end{pmatrix} \qquad G = \begin{pmatrix} \rho v \\ \rho uv \\ \rho v^2 + p \\ v(e + p) \end{pmatrix}$$

and

$$p = (\gamma - 1)\left[e - \frac{\rho}{2}(u^2 + v^2)\right] \tag{6b}$$

Here u and v are the Cartesian components of fluid velocity; ρ is the density, p is the pressure, e is the total energy of the fluid per unit volume, terms F and G are the flux terms along the x and y directions, and γ is the ratio of specific heats; the subscripts denote differentiation with respect to time, and spatial coordinates x and y.

The body-fitted coordinate system (ξ, η, τ) is related to the Cartesian coordinates (x, y, t) (fig. 2), according to the following one-to-one relationship:

$$\xi = \xi(x, y, t) \qquad \eta = \eta(x, y, t) \qquad \tau = ta_1/2b \tag{7}$$

In the (ξ, η, τ) coordinate system, the two-dimensional unsteady Euler equations may be written as

$$\hat{q}_\tau + \hat{F}_\xi + \hat{G}_\eta = 0 \tag{8a}$$

where

$$\hat{q} = \bar{J}^{-1}\begin{pmatrix} \rho \\ \rho u \\ \rho v \\ e \end{pmatrix} \tag{8b}$$

The Jacobian of the transformation J is given by

$$J = \xi_x \eta_y - \xi_y \eta_x = (x_\xi y_\eta - x_\eta y_\xi)^{-1} \tag{9}$$

and the metrics of the transformation are given by the relationships:

$$\xi_x = J y_\eta; \qquad \xi_y = -J x_\eta; \qquad \eta_x = -J y_\xi; \qquad \eta_y = J x_\xi \tag{10}$$

Once a grid has been constructed, the metrics of the transformation are evaluated numerically. Standard central differences are used to compute the quantities such as x_ξ, y_ξ, etc., and these quantities in turn are used in equations (9) and (10) to compute ξ_x, ξ_y, etc.

Since equation (8) is highly nonlinear, a stable and efficient solution procedure is required. In the present work, the Beam-Warming algorithm (ref. 16) is used with modifications noted by Sankar and Tang (ref. 15). Artificial dissipation is added in both directions of the computational plane to increase solution stability. The solution is second-order accurate in space and first order accurate in time.

Grids.—The flow solver uses a C-grid generated using the GRAPE (GRids about Airfoils using Poisson's Equation) code (ref. 17) with modifications for cascade geometries (ref. 11). Multiple blade grids are constructed by stacking the individual C-grids for each blade. The flow solver works with one grid at a time. For a cascade geometry, the location of the grid points on the interface boundary must be known to pass information to adjacent grids across this common boundary (fig. 2(c)). In order to avoid difficult interpolations and to facilitate the application of boundary conditions at the interface, it is desirable that grid points along the outer boundaries of adjacent grids line up exactly. This is achieved by the stacking of the individual C-grids generated using the GRAPE code.

The grids are generated only once around the steady positions of the airfoils. Since the airfoils move during the computation (unsteady solution), it is necessary to move the surrounding grid too. A simple rigid body rotation of the grid (as is commonly done for isolated airfoils) is unsuitable for a cascade. A special procedure is required to keep the outer boundary of the grid fixed while allowing the airfoil to move.

A deforming grid technique (ref. 12) is used in this analysis to locate the position of the grid points as a function of time. The inner boundary follows the blade motion, while the outer boundary remains fixed in space (figs. 2(a) and 3). All interior grid lines connecting the inner and outer boundaries are allowed to deform. The amount of deformation is a function of the distance from the surface of the airfoils together with a weighting function. The displacement of a grid point (i,j) is defined as:

$$\Delta x_{i,j} = w_{i,j} \, \Delta x'_{i,j} \tag{11a}$$

$$\Delta y_{i,j} = w_{i,j} \, \Delta y'_{i,j} \tag{11b}$$

where $\Delta x_{i,j}$ and $\Delta y_{i,j}$ are the spatial displacements of grid point (i,j), and $\Delta x'_{i,j}$ and $\Delta y'_{i,j}$ are the spatial displacements of grid point (i,j) over one time step assuming that the entire grid is moved as a rigid body. The weighting function, $w_{i,j}$ is defined as:

$$w_{i,j} = \left| \frac{s_{i,j}}{s_{i,jmax}} - 1 \right| \tag{12}$$

where $s_{i,j}$ is the arc length from the airfoil surface ($j = 1$) to some grid point along a $i =$ constant grid line, and $j = jmax$ corresponds to the outer boundary grid line. From equations (11) and (12), it can be seen that grid points on the inner boundary ($s_{i,j} = 0$) give $w_{i,j} = 1$, which means the airfoil surface follows the rigid body motion of the blade. Conversely, the grid points on the outer boundary give $w_{i,j} = 0$ and the positions of these grid points remain fixed at the initial specified locations. The interior grid points shear in space relative to the initial grid as $w_{i,j}$ varies between 0 and 1. The grid velocities can be easily found by dividing the grid deformation by the time step value. Using this deforming grid approach, the metrics must be recalculated at each time step.

Boundary conditions.—The present flow solver independently solves the flow equations for each grid around a blade and uses interface boundary conditions to model the cascade effects. Ghost points are assigned at the first interior grid line ($j = jmax - 1$) and are used by the adjacent grid. Although it is tempting to use the most current flow information as it becomes available from the integration scheme, it is important to only use flow information from the same time step across the interface boundaries. This eliminates possible time inaccuracy in multiple blade solutions due to the particular sequence in which individual grid solutions are obtained. The metric data are also forced to be continuous along the interface boundaries. This procedure essentially makes the blade-to-blade interface boundaries invisible to the flow solution. Periodic boundary conditions (explained in the next section) are applied at the lower and upper boundaries of the cascade (fig. 2(c)).

The remaining boundary conditions include those at the inlet and exit planes, the blade surfaces and the slits aft of the airfoils (fig. 2). At the inlet the flow variables (density, two velocity components, and pressure) are specified to be uniform. At the exit these flow variables are extrapolated from the interior by using a simple first order model. These boundary conditions are valid for supersonic flow at the inlet and exit. Solid wall boundary conditions are applied along the airfoil surface and the flow variables are averaged across the slit aft of the airfoil.

Periodic boundary conditions and interblade phase angle (σ).—The flow through a two-dimensional rectilinear cascade is a model for the flow through a N bladed rotor or stator of a turbomachine. Hence, there exists a fundamental spatial periodicity across the ends (in the direction of the stagger line) of the cascade consisting of N blades. Periodic boundary conditions can, therefore, be applied at the upper and lower boundaries of the N blade cascade; the periodic boundary conditions constrain the flow variables to be equal at corresponding points on the two boundaries. However, under certain circumstances it is possible to apply the periodicity condition across a much smaller domain, as will be explained in this section. Clearly, this can result in a substantial saving of computational resources.

For steady flow through a stationary cascade, blade-to-blade periodicity of flow variables exists naturally. Hence, the periodic boundary conditions are applied at the upper and lower boundaries of a single grid; that is, the flow variables are required to have identical values at corresponding points on the outer boundary of a *single grid* (fig. 4(a)). The computations are performed on only one grid rather than on N grids since the flow field would be reproduced identically in the remaining grids.

For unsteady flows in which all blades have identical motions, the blade-to-blade periodicity of steady flows is preserved. Hence, the periodic boundary conditions can again be applied at the upper and lower boundaries of a *single grid.*

For unsteady flows in which all blades have the same periodic motion, except for a constant time-lag between adjacent blades, the periodicity condition can be applied across a group containing between 1 and N *grids.* Consider a case where all blades move in a simple harmonic motion of the form $\sin(\omega t)$, except for a constant time-lag between adjacent blades. The time-lag can be represented in terms of the interblade phase angle (σ) so that the motion of the N blades is of the form $\sin(\omega t)$, $\sin(\omega t + \sigma)$, $\sin(\omega t + 2\sigma)$, etc. The interblade phase angle cannot assume arbitrary values, but is restricted to N discrete values, $\sigma = 2\pi n/N$, n = 0, 1, 2,. . ., N - 1, where N is the number of blades of the cascade. This is referred to as Lane's criterion (ref. 18). For the motion described, it is possible to apply the periodicity conditions across a group of grids; the number of grids in the group is between 1 and N, depending on the value of the interblade phase angle. For example, an interblade phase angle of 180° requires a group with two grids (fig. 4(b)), 90° requires four grids (fig. 4(c)), etc. The number of grids in a group (NGG) for a given σ is given by

$$\text{NGG} = \text{smallest integer}[360/\sigma,\ 360/(360 - \sigma),\ \text{N}]$$

or

$$\text{NGG} = \text{smallest integer}[\text{N/n},\ \text{N}/(\text{N} - \text{n}),\ \text{N}]$$

The use of NGG grids in the computation instead of N grids represents a saving in computational effort while providing the correct treatment of boundary conditions for this case of simple harmonic motion with constant interblade phase angle. This method of using the required number of grids *(NGG)* for a given interblade phase angle is referred to as the multipassage approach (ref. 19).

Clearly, a group with the number of grids equal to the number of blades on the rotor can be used to compute all the interblade phase angles that arise in flutter calculations (fig. 4(d)). However, the use of more than NGG grids for a particular value of σ would require additional computational effort without providing any additional information; the flow field in the group containing NGG grids would be reproduced periodically in the remaining (N - NGG) grids. It can also be pointed out that one can use more than one group in the computation, so that the total number of grids is between NGG and N. For example, for an eight-bladed rotor, and for $\sigma = 180°$, one can use two, four, six, or eight grids in the computation, with periodic boundary conditions applied across the corresponding number of grids. It can be verified that the solution in the basic group containing two grids (NGG = 2) will be same in all the cases, and this solution will be reproduced in the additional grids being used in the last three cases.

Periodic boundary conditions and time response calculations.—The preceding discussion was based on the assumption of periodic blade motions. In the time integration method, the blade motion is not known in advance, and is in general, oscillatory but not periodic. Hence, no fixed frequency or interblade phase angle can be identified. The term "interblade phase angle" that will be used in connection with the time integration method refers to the interblade phase angle of the forced simple harmonic motion that is used to provide the appropriate initial conditions to the time integration method.

The time integration calculations would normally be performed over N grids. For a tuned cascade, for which all blades are identical, the governing aeroelastic equation for each blade (eq. (1)) is the same. Hence, the response of the blades can differ only if the initial conditions are different. For example, $\sigma = 0°$ (for the forced motion) will result in all blades having identical responses. In this case it is sufficient to calculate the response of only one blade. Similarly, for $\sigma = 180°$, it is sufficient to calculate the response of only two blades (using two grids), since the response of all the remaining blades will be the same as that of either one of these blades. It can therefore be seen that the concept of identifying a group containing NGG grids, across which periodicity can be imposed, remains valid for the time integration method. This also means that for a given interblade phase angle, only NGG aeroelastic equations (eq. (4)) need to be solved.

It has been pointed out in reference 12 that for supersonic axial flow the computational domain of the flow field can be reduced by inspecting the shock structure through the cascade. The disturbances generated inside the Mach cone of the leading edge do not influence the flow outside the cone, which means that only a few blades (which fall within the Mach cone of the reference blade) need to be considered in the solution for any interblade phase angle. It was also noted that only the aerodynamic loads on the reference blade are valid for the specified interblade phase angle. This procedure works quite well when the blade motion is simple harmonic with constant interblade phase angle, since the loads on the other blades can be calculated once those on the reference blade are known. However, in time-domain aeroelastic analysis, the aerodynamic loads on all blades cannot be related to the loads on the reference blade, even for a tuned cascade. In this situation, the computations must be made on a group of blades depending on the interblade phase angle. By doing this the forces on all the blades and the aeroelastic analysis will be accurate.

Procedure for aeroelastic analysis.—In general, the aeroelastic equation (eq. (4)) is integrated in time for each blade independently. As mentioned earlier, the number of blades used in the calculation depends on the interblade phase angle; the minimum number of blades required is NGG. The time integration of the aeroelastic equations can be started from prescribed initial conditions, $\alpha(0)$ and $\alpha'(0)$ for each blade or from initial forced harmonic motion of three to four cycles. In the present study, the latter is followed. First, the aerodynamic solution is obtained for three cycles of forced oscillation for given flow conditions and interblade phase angle with an assumed reduced frequency. Then, with the motion and the forces (in this case the moment) at the end of the third cycle as the initial conditions, the aeroelastic equations are integrated (ref. 20). This procedure has three advantages:

(1) The results can be checked by comparison with those obtained in reference 12.

(2) The forces can be Fourier decomposed, and a frequency domain flutter analysis can be performed (ref. 21).

(3) It provides the correct initial values for $\alpha(0)$ and $\alpha'(0)$ that correspond to a specified interblade phase angle of forced motion.

To begin the response calculations, a value of nondimensional speed V^* (eq. (4)) is assumed. Variation of the blade motion with time is plotted and stability is assessed from the response. If the response grows with time, the value of V^* is reduced and vice versa. The aeroelastic equations are then integrated again. The process is repeated until a value of V^* is found for which the response is neutrally stable; this value of V^* is the flutter speed.

Programming aspects.—Multiblade solutions for oscillating cascades are obtained by generating grids for each blade. These grids have the same outer boundary shape but different airfoil positions. The

solver generates these grids before the unsteady calculation begins by deforming the mean flow grid for one blade through a cycle of forced oscillation and storing the grids that occur at multiples of the desired interblade phase angle. For example, when $\sigma = 90°$, four grids (NGG = 4) need to be assembled with a blade to blade phase angle of 90° (fig. 4(c)). With the forced oscillation motion assumed to be given by $\alpha = \alpha_0 + \alpha_1 \sin(\omega t)$, where α_0 and α_1 are the mean and amplitude of oscillation, and ω is the frequency of oscillation, the grid from the mean flow solution is used for the first blade ($\omega t = 0$). The grids for the remaining three blades are found by deforming the mean flow grid through one cycle of oscillation and storing the grid coordinates when $\omega t = 90°$, 180°, and 270°. The solver numbers the blades and stacks the grids to give one group of grids containing four blades. This group is then used as the initial grid for the unsteady solution, where it is deformed for the oscillating cascade using the method described in the previous section.

RESULTS AND DISCUSSION

The response curves (variations of pitching amplitude with time) are presented for a flat plate cascade and for airfoil sections of a supersonic throughflow fan rotor and stator undergoing pitching motion. The responses are obtained by integrating the aeroelastic equations (eq. (4)) for each blade. The flutter speeds are calculated from the response data. As mentioned earlier, first the blades are oscillated in forced motion and then equation (4) is advanced in time. Flutter predictions from frequency domain solutions are also presented for comparison.

The results are presented for the following combinations of parameters (ref. 8): As previously described, a C-grid is generated for each blade by using GRAPE code.

(1) flat plate airfoil and rotor airfoil
gap-to-chord ratio, g/c = 0.311
stagger angle, $\theta = 28°$
mass ratio, $\mu = 456$
radius of gyration (mid chord), $r_\alpha = 0.4311$
computational grid, 199×22 ($\xi \times \eta$)

(2) stator airfoil
gap-to-chord ratio, g/c = 0.295
stagger angle, $\theta = 11.7°$
mass ratio, $\mu = 456$
radius of gyration (mid chord), $r_\alpha = 0.4311$
computational grid, 225×22 ($\xi \times \eta$)

A frequency domain flutter analysis based on linear theory for supersonic axial flow (ref. 8), indicated that for the structural parameters (μ, r_α) and cascade parameters (θ, g/c) selected here, the instability was essentially a pitching motion instability. This suggests that the analysis developed here with only pitching motion is sufficient for the present problem. All the calculations are done on a CRAY Y-MP computer. The solution takes about 2.11×10^{-5} CPU sec per time step per grid point per blade and requires about 1.8 MW storage. A typical response calculation with two blades requires about 400 CPU sec.

Flat Plate Cascade

The geometry of the flat plate cascade is derived from the SSTF rotor. However, calculations have been performed for arbitrary values of interblade phase angle, not limited to the values given by Lane's criterion referred earlier. Results are presented for $\theta = 28°$ and inlet flow angle (β) of 28°, giving a steady angle of attack (α_0) of 0°. A thickness ratio of 0.5 percent is used and the leading and trailing edges are rounded to aid in the generation of the C-grid (fig. 5). The steady pressure distribution obtained for this flow condition is presented in reference 12.

The variation of the imaginary part of the moment coefficient ($Im\{c_m\}$) with interblade phase angle (σ) is presented in figure 6 for two values of reduced frequency (k_b); the steady flow Mach number at the inlet section is 2.61. These results are obtained by forcing the flat plate cascade in harmonic motion for a given σ and reduced frequency k_b. The moment coefficient is calculated from the pressure distribution and Fourier transformed to get the real and imaginary coefficients. The pitching axis is at 30 percent of chord ($x'/c = 0.3$), which was found to be the best location for causing flutter in reference 8. The frequency domain flutter solution is obtained as a part of the time integration procedure as mentioned in the "procedure for aeroelastic analysis" section. Note that for a pitching airfoil, the $Im\{c_m\}$ indicates the stability: positive values indicate unstable motion and vice versa. Also, note that the reduced frequency (k_b), used in the analysis is based on semichord, b.

From figure 6, it can be seen that for $k_b = 1.00$, the $Im\{c_m\}$ is positive for σ between 110° and 260°; for $k_b = 1.50$, $Im\{c_m\}$ is negative for all values of σ. It can be seen that the interblade phase angle with the highest imaginary moment coefficient is 180°; i.e., the critical interblade phase angle for this cascade is 180°. The value of reduced frequency at which $Im\{c_m\}$ becomes zero (neutrally stable motion), for $\sigma = 180°$, is calculated by linear interpolation as $k_b = 1.4$.

To calculate the neutrally stable condition in the time domain analysis, the response for $\sigma = 180°$ is obtained for two values of nondimensional speed, $V^*(=V_1/b\omega_\alpha)$ (eq. (4)), one for a low V^* (converging oscillations) and the other for a high V^* (diverging oscillations). The flutter speed corresponding to neutrally stable oscillations (zero damping) is calculated from these two responses by linear interpolation; this result is then compared with the frequency domain solution obtained above. Note that at flutter V^* and k_b are related by $k_b = (1/V^*)(\omega/\omega_\alpha)$ as given in equation (5); here ω_α is the frequency of the typical section in pitch.

The variation of the pitching amplitude with time is shown in figure 7 for $\sigma = 180°$. A group consisting of two grids is used in the numerical calculations. The response calculations for two values of V^* for blade 1 (corresponding to grid 1) are shown in figure 7(a). The response for $V^* = 0.6$ shows converging oscillations, where as for $V^* = 1.0$, it shows diverging oscillations. The calculated flutter speed for zero damping is $V^* = 0.762$ and $(\omega/\omega_\alpha) = 0.995$. The value of k_b calculated from the response and equation (5) is 1.311, which is 7 percent lower than the one obtained previously from frequency domain solution.

Figure 7(b) shows the response obtained from calculations from blade 2 (corresponding to grid 2). Comparing the responses in figures 7(a) and (b), it can be seen that both blades 1 and 2 show the same response differing only by the phase angle of the initial forced motion. This indicates that the effect of the interblade phase angle is accurately accounted for while integrating the aeroelastic equations. The calculations were repeated with a group containing four grids. Identical responses were obtained (not shown) for the alternate blades, indicating that a group consisting of two grids is enough for $\sigma = 180°$. In order to further validate the time integration method, responses were calculated at other interblade phase angles and correlated with the frequency domain results. From figure 6 it can be seen that the flat plate cascade in pitching motion was stable for $\sigma = 0°$, 90°, and 300° for $k_b = 1.0$. Since (ω/ω_α) is nearly equal to one for this case, it is necessary only to show that the corresponding responses at $\sigma = 0°$, 90°, and 300° are stable for $V^* = 1.0$. For these interblade phase angles, groups consisting of one, four, and six grids, respectively, are used. Figure 8(a) shows the responses obtained for all the four interblade phase angles studied here, namely $\sigma = 0°$, 90°, 180°, and 300°. The variation of the imaginary moment coefficient with σ (from fig. 6) is repeated in figure 8(b). It can be seen that for $\sigma = 0°$, 90°, and 300°, the response is stable whereas for $\sigma = 180°$, it is unstable. This indicates that for $\sigma = 0°$, 90°, and 300°, a higher V^* would be required for unstable oscillations. This is consistent with observations in the frequency domain analysis for $k_b = 1.0$ as shown in figure 8(b).

From the above calculations, it is concluded that the aeroelastic equations are being correctly integrated and the effect of interblade phase angle is being accurately accounted for in the time integration method.

SSTF Airfoil Cascade

Having established that the time integration method is properly implemented for cascade analysis, the flutter speeds of two airfoil sections are calculated in both frequency and time domains and the results are correlated. One of the airfoils corresponds to the rotor and the other to the stator section near the midspan of a supersonic throughflow fan. Additional design parameters of the SSTF fan can be found in reference 3.

Rotor section.—The SSTF rotor airfoil section is about 5 percent thick, and has a chord of 4.065 in. This corresponds to a midspan span location on a compressor blade design at NASA Lewis. The solutions are obtained for $\beta = 36°$ and $\theta = 28°$, giving a steady angle of attack (α_0) of 8° (fig. 1(a)). The steady, static pressure obtained for this flow condition is presented in figure 9(a) and is compared with that obtained in reference 11. Both show a good qualitative trend. However, the present solver predicts the shock to be located about 10 percent downstream of the position predicted by reference 11. The discrepancy may be due to viscous and quasi-three-dimensional effects that are included in the analysis of reference 11, in addition to different grid sizes.

The rotor has 44 blades. Lane's criterion indicates that the rotor can become unstable in any of the possible 58 interblade phase angle modes. Therefore, the flutter analysis should be performed for 58 interblade phase angles, some of which may require up to 58 passages (grids). Fortunately, for this supersonic throughflow cascade, the critical interblade phase angle lies between 180° and 230° (ref. 8); this allows the calculations to be performed with a small number of passages (NGG = 2 to 8).

For the results that follow, a frequency domain flutter analysis was done first. The time domain solution was then obtained for selected interblade phase angles and the results were correlated with the frequency domain results. The variation of imaginary moment coefficient with interblade phase angle is shown in figure 9(b) for two values of reduced frequency. The moment is taken about a point near the midchord. From figure 9(b), it can be seen that for $k_b = 0.25$, the $\mathrm{Im}\{c_m\}$ is positive for σ between 110° and 260°; for $k_b = 0.5$, $\mathrm{Im}\{c_m\}$ is negative for all values of σ. The critical interblade phase angle moves from 180° for $k_b = 0.25°$ to 230° for $k_b = 0.5$. At flutter, the critical interblade phase angle (for which the $\mathrm{Im}\{c_m\}$ is the greatest) is 180° and the calculated value of k_b at which $\mathrm{Im}\{c_m\}$ becomes zero is 0.29.

Again, as was done for the flat plate cascade, the response for $\sigma = 180°$ is obtained for two values of nondimensional speed (V^*). A group consisting of two grids is used in the numerical calculations. The responses for two values of V^* from blade 1 (solid lines) are shown in figure 10. Response for $V^* = 2.8$ shows converging oscillations, whereas for $V^* = 3.0$, it shows diverging oscillations. The calculated flutter speed is $V^* = 2.915$ and $(\omega/\omega_\alpha) = 0.877$; the value of k_b calculated from equation (5) is 0.301, which is 3.8 percent higher compared to the value obtained from the frequency domain solution. Figure 10 also shows the response calculation from blade 2 (dotted lines) for the same values of V^*. It can be seen that the responses of blades 1 and 2 have the same amplitude but differ in phase angle.

Compared to the flat plate case studied in the previous section, the loaded SSTF airfoil becomes unstable at a higher flutter speed. Also, the response curves show the influence of steady aerodynamic loading on the response. In the case of the flat plate, the steady aerodynamic load is zero, and the aero-

elastic response oscillated about a mean of zero. However, for the airfoil section, the steady loading is not zero and as soon as the forced motion ends the mean motion changes to a value dictated by the steady aerodynamic loading. Nevertheless, after the transients due to steady loading have decayed, both the blades maintain the same interblade phase angle.

Stator section: The stator has 52 blades. The airfoil section of the stator is about 5 percent thick, and has a chord of 3.49 in. This corresponds to a midspan location on a compressor blade designed at NASA Lewis. The solutions are obtained for $\beta = 23.3°$ and $\theta = 11.7°$, giving a steady angle of attack (α_0) of 11.6° (fig. 1(b)).

The variation of imaginary moment coefficient with interblade phase angle is shown in figure 11 for two values of reduced frequency at an inlet Mach number of $M_1 = 2.72$. The moment is taken about a point near the midchord point. It can be seen that for $k_b = 0.3$, the $\mathrm{Im}\{c_m\}$ is positive for σ between 110° and 260°; for $k_b = 0.4$, $\mathrm{Im}\{c_m\}$ is negative for all values of σ. The value of k_b, at which $\mathrm{Im}\{c_m\}$ becomes zero is 0.389. The critical interblade phase angle is 180°.

As was done for the rotor airfoil section cascade, first the response for $\sigma = 180°$ is obtained for two values of nondimensional speed (V^*). The responses are shown in figure 12. Again, a group consisting of two grids is used in the numerical calculations. The response for two values of V^* from blade 1 (solid lines) are shown in figure 12. Response for $V^* = 2.0$ shows converging oscillations, where as for $V^* = 2.5$, it shows diverging oscillations. The calculated flutter speed is $V^* = 2.30$ and $(\omega/\omega_\alpha) = 0.902$. The calculated k_b is 0.392, which is within 1 percent of the value obtained from frequency domain solution. Figure 12 also shows the response calculations from blade 2 (dotted lines) for the same values of V^*. It can be seen that the responses of blades 1 and 2 show the same amplitude but differ in phase angle. In figure 12, it is also seen that the steady loading causes the response to oscillate about a new mean position after the forced motion ends.

Additional time domain response calculations (not shown here) for rotor and stator airfoil sections also showed the behavior predicted by frequency domain flutter calculations for other interblade phase angles.

CONCLUDING REMARKS

A time response procedure is developed for prediction of flutter of a two-dimensional cascade in supersonic axial flow. The analysis is based on a typical section structural model and uses a finite difference code based on the Euler equations. The initial condition used to start the time integration procedure is a harmonic motion of each blade with an interblade phase angle.

The predicted flutter speeds correlated well with those obtained from a frequency domain analysis. The expected behavior is reproduced by the time integration method for the interblade phase angles considered. The calculations for the loaded airfoil sections showed higher flutter speeds compared to the flat plate cascade. This shows the importance of including the effects of shape, thickness and loading in the analysis.

An alternative procedure for simultaneously calculating the response in all interblade phase angle modes is under consideration; this consists of using general (random) initial conditions. This eliminates the need to of calculate responses for each interblade phase angle mode separately, as done in the present paper. It may provide substantial saving in computational time and this procedure is being investigated at the present time.

ACKNOWLEDGMENT

The authors would like to thank Professor Marc Williams of Purdue University for many helpful suggestions.

REFERENCES

1. Strack, W.C.; and Morris, Jr., S.J.: The Challenges and Opportunities of Supersonic Transport Propulsion Technology. NASA TM-100921, 1988.

2. Franciscus, L.C.: The Supersonic Through-Flow Turbofan for High Mach Propulsion. AIAA Paper 87-2050, 1987.

3. Schmidt, J.F. et al.: Supersonic Through-Flow Fan Design. NASA TM-88908, 1987.

4. Wood, J.R. et al.: Application of Advanced Computational Codes in the Design of an Experiment for a Supersonic Through Flow Fan Rotor. ASME Paper 87-GT-160, 1987.

5. Nishiyama, T.; and Kikuchi, M.: Theoretical Analysis for Unsteady Characteristics of Oscillating Cascade Aerofoils in Supersonic Flows. The Technol. Rep., Tohoku Univ., vol. 38, no. 2, 1973, pp. 565-597.

6. Nagashima, T.; and Whitehead, D.S.: Linearized Supersonic Unsteady Flow in Cascades. British Aeronautical Research Council, ARC-R/M-3811, 1977.

7. Platzer, M.F.; and Chalkley, Lt. H.G.: Theoretical Investigation of Supersonic Cascade Flutter and Related Interference Problems. AIAA Paper 72-377, 1972.

8. Kielb, R.E.; and Ramsey, J.K.: Flutter of a Fan Blade in Supersonic Axial Flow. J. Turbomach., vol. 111, Oct. 1989, pp. 462-467.

9. Lane, F.: Supersonic Flow Past an Oscillating Cascade with Supersonic Leading Edge Locus. J. Aeronaut. Sci., vol. 24, 1957, pp. 65-66.

10. Kaza, K.R.V.; and Kielb, R.E.: Flutter and Response of a Mistuned Cascade in Incompressible Flow. AIAA J., vol. 20, no. 8, Aug. 1982, pp. 1120-1127.

11. Chima, R.V.: Explicit Multi-Grid Algorithm for Quasi Three-Dimensional Viscous Flows in Turbomachinery. J. Propuls. Power, vol. 3, no. 5, Sept.-Oct. 1987, pp. 397-405.

12. Huff, D.L.; and Reddy, T.S.R.: Numerical Analysis of Supersonic Flow Through Oscillating Cascade Sections by Using a Deforming Grid. AIAA Paper 89-2805, 1989.

13. Reddy, T.S.R.; Srivastava, R.; and Kaza, K.R.V.: The Effects of Rotational Flow, Viscosity, Thickness, and Shape on Transonic Flutter Dip Phenomena. NASA TM-100811, 1988 (also, AIAA Paper 88-2348, 1988).

14. Bathe, K.-J.; and Wilson, E.L.: Numerical Methods in Finite Element Analysis. Prentice-Hall, Englewood Cliffs, NJ, 1976.

15. Sankar, L.N.; and Tang, W.: Numerical Solution of Unsteady Viscous Flow Past Rotor Sections. AIAA Paper 85-0129, 1985.

16. Beam, R.M.; and Warming, R.F.: An Implicit Factored Scheme for the Compressible Navier-Stokes Equations. AIAA J., vol. 16, no. 4, Apr. 1978, pp. 393-402.

17. Sorenson, R.L.: A Computer Program to Generate Two-Dimensional Grids About Airfoils and Other Shapes by the Use of Possion's Equation. NASA TM-81198, 1980.

18. Lane, F.: System Mode Shapes in the Flutter of Compressor Blade Rows. J. Aeronaut. Sci., vol. 23, Jan. 1956, pp. 54-66.

19. Huff, D.L.: Numerical Analysis of Flow Through Oscillating Cascade Sections. AIAA Paper 89-0437, 1989 (also, NASA TM-101417, 1989).

20. Ballhaus, W.F.; and Goorjian, P.M.: Computation of Unsteady, Transonic Flows by the Indicial Method. AIAA J., vol. 16, no. 2, 1978, pp. 117-124.

21. Bakhle, M.A.; Keith, Jr., T.G.; and Kaza, K.R.V.: Application of a Full-Potential Solver to Bending-Torsion Flutter in Cascades. AIAA Paper 89-1386, 1989.

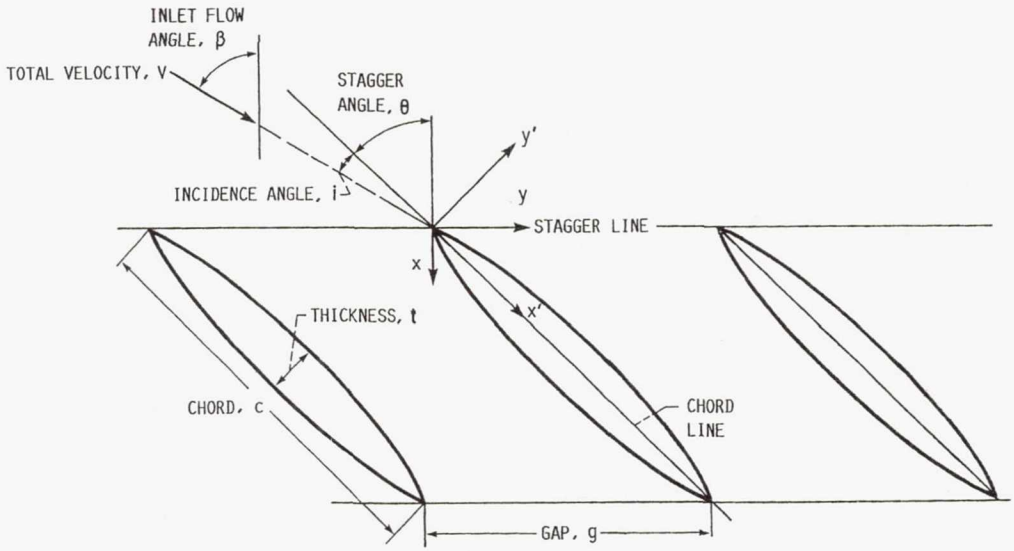

(a) Cascade geometry.

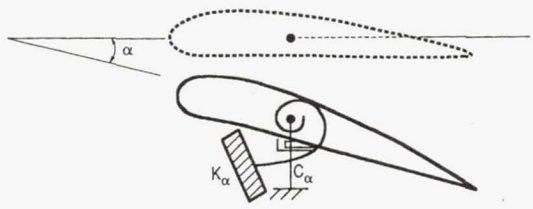

(b) Typical section model.

Figure 1.—Cascade geometry and typical section model.

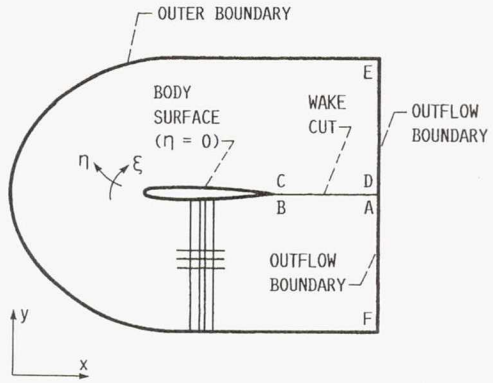

(a) C-grid in physical plane.

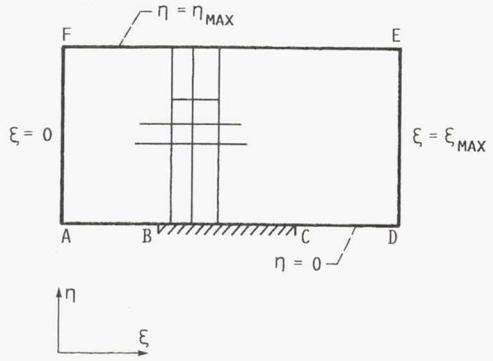

(b) C-grid in computational plane.

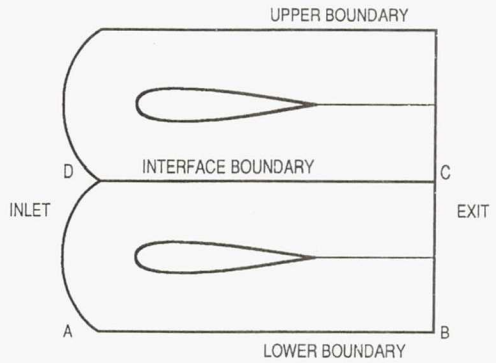

(c) Grid boundary definitions.

Figure 2.—C-grid in physical and computational planes and grid boundary definitions.

(a) Undeformed grid.

(b) Deformed grid.

Figure 3.—Deforming grid technique with exaggerated motion.

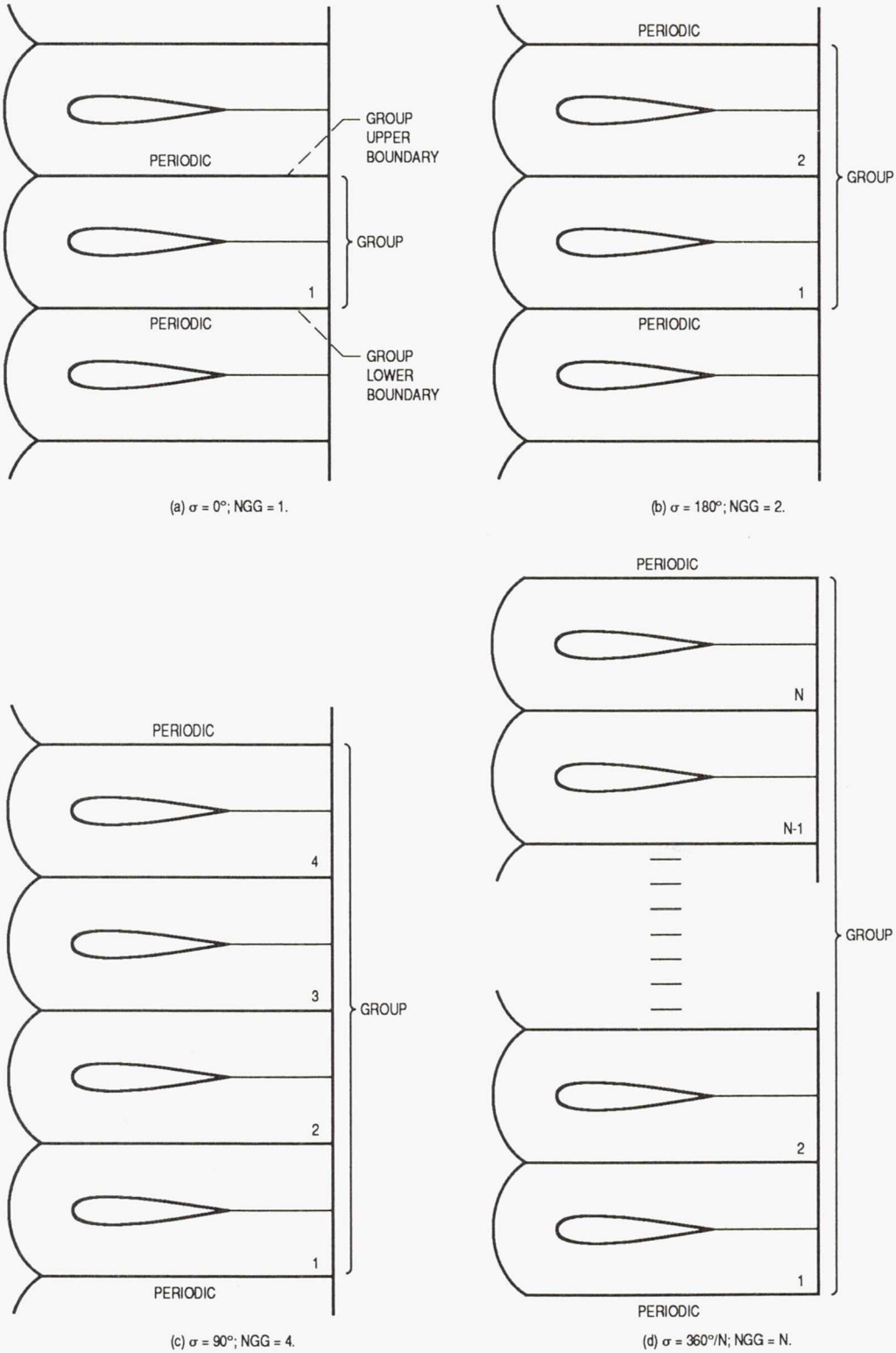

(a) $\sigma = 0°$; NGG = 1.

(b) $\sigma = 180°$; NGG = 2.

(c) $\sigma = 90°$; NGG = 4.

(d) $\sigma = 360°/N$; NGG = N.

Figure 4.—Relation between minimum number of grids per group (NGG) and interblade phase angle (σ) for an N bladed cascade.

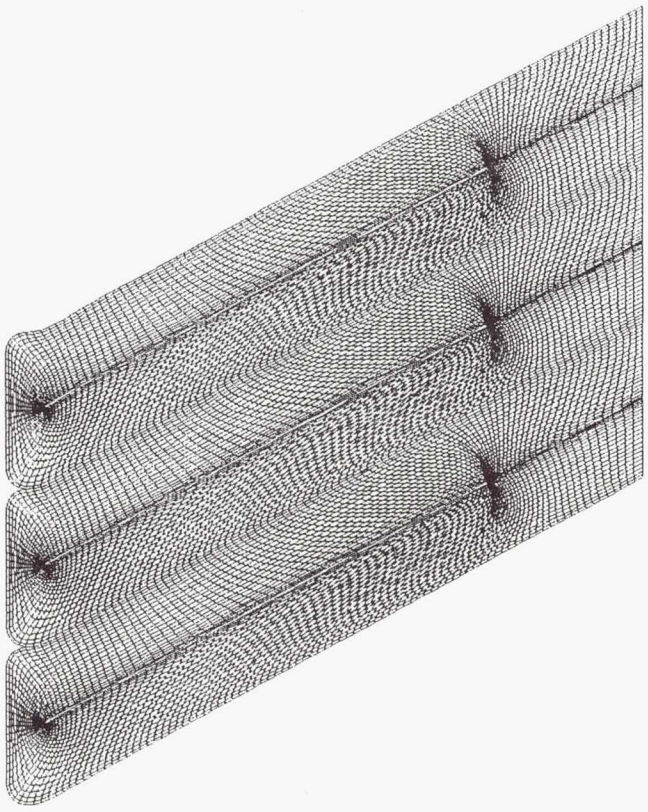

(a) Global grid.

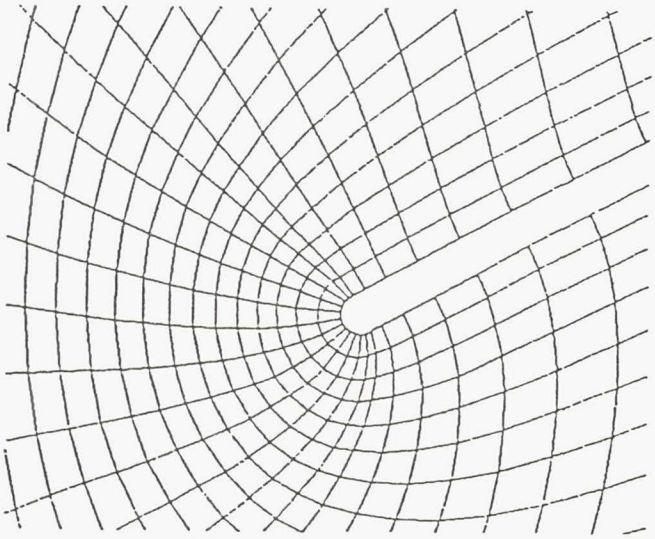

(b) Enlarged view of leading-edge region.

Figure 5.—Grid for flat plate cascade.

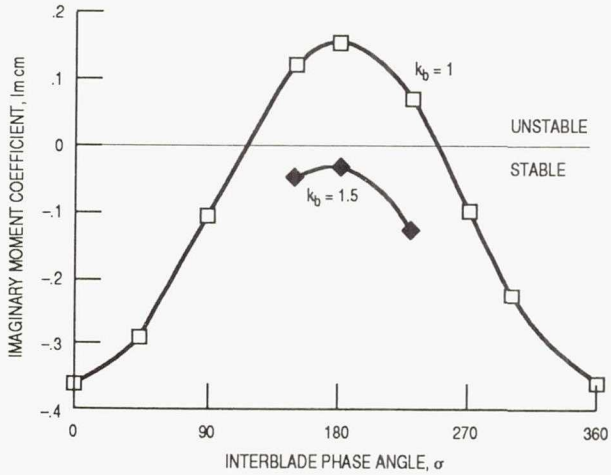

Figure 6.—Imaginary part of moment coefficient about $x'/c = 0.3$ versus interblade phase angle; flat plate cascade; inlet Mach number $M_1 = 2.61$; stagger angle $\theta = 28°$; inlet flow angle $\beta = 28°$; gap-to-chord ratio $g/c = 0.311$; pitching displacement $\alpha = 0.1 \sin(\omega t)$.

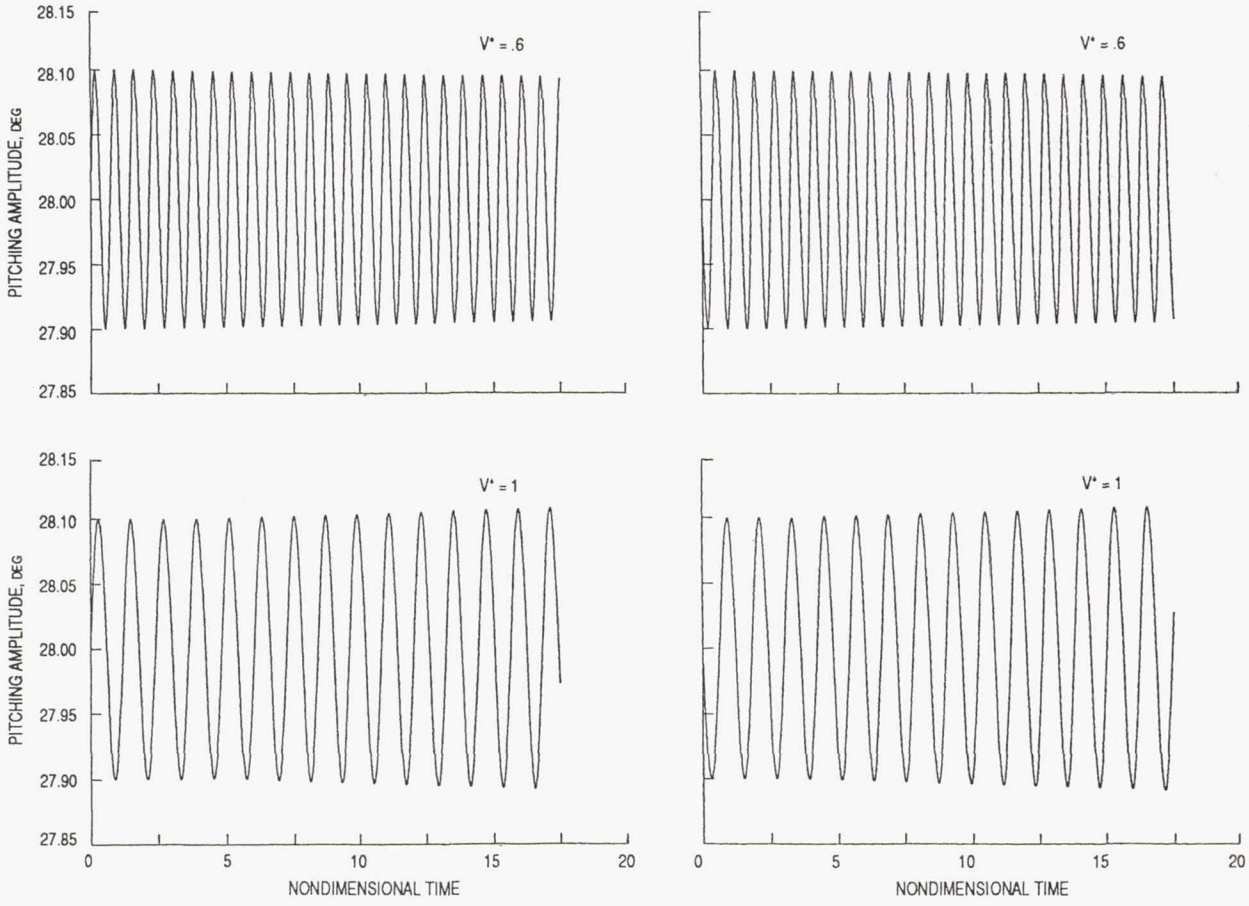

(a) Blade 1.

(b) Blade 2.

Figure 7.—Response of flat plate cascade (parameters same as for Fig. 6; interblade phase angle $\sigma = 180°$).

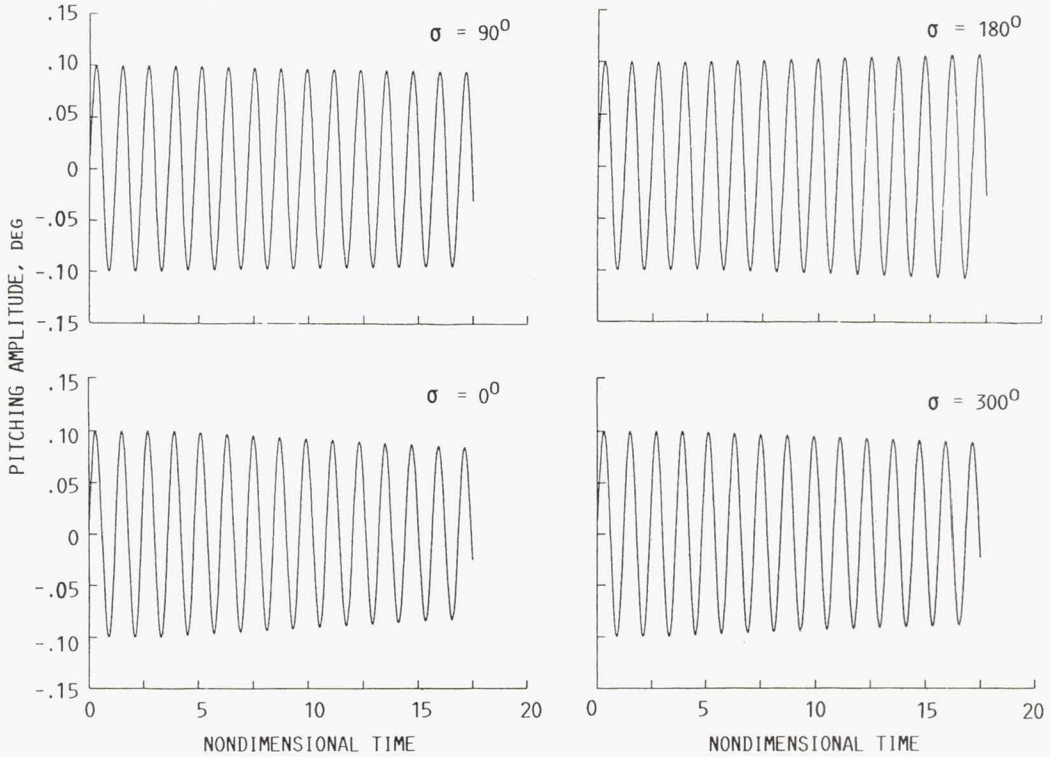

(a) Response of flat plate cascade for interblade angles of 0°, 90°, 180°, and 300° (parameters same as for Fig. 6; blade 1, $V^* = 1.0$).

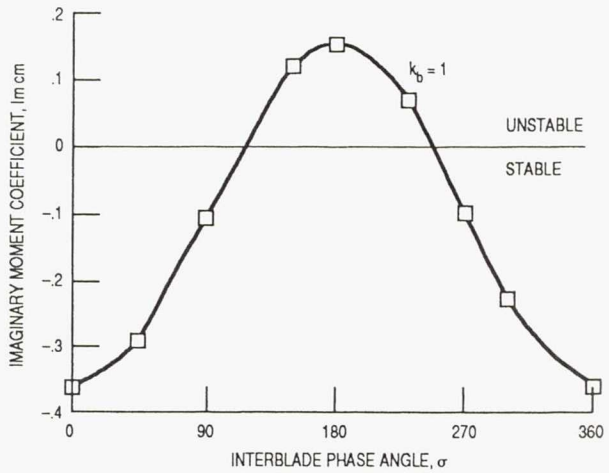

(b) Imaginary part of moment coefficient about $x'/c = 0.3$ versus σ, $k_b = 1.0$.

Figure 8.—Response of flat plate cascade for all four interblade phase angles and variation of imaginary moment coefficient with interblade phase angle (σ).

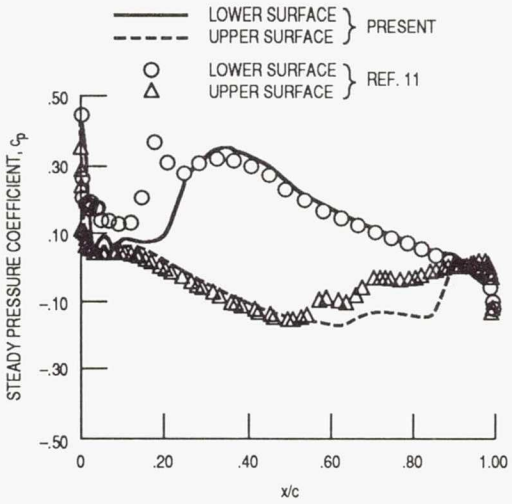

(a) Steady pressure coefficient distribution for rotor airfoil configuration.

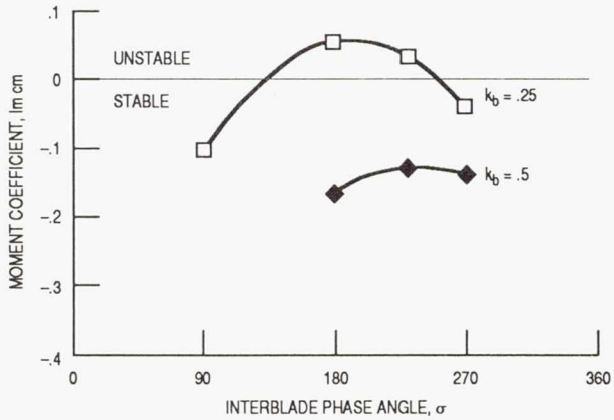

(b) Imaginary part of moment coefficient versus σ (rotor section airfoil; parameters same as for Fig. 6, except inlet flow angle β = 36°.

Figure 9.—Steady pressure coefficient distribution for rotor airfoil configuration and variation of imaginary moment coefficient with interblade phase angle (σ).

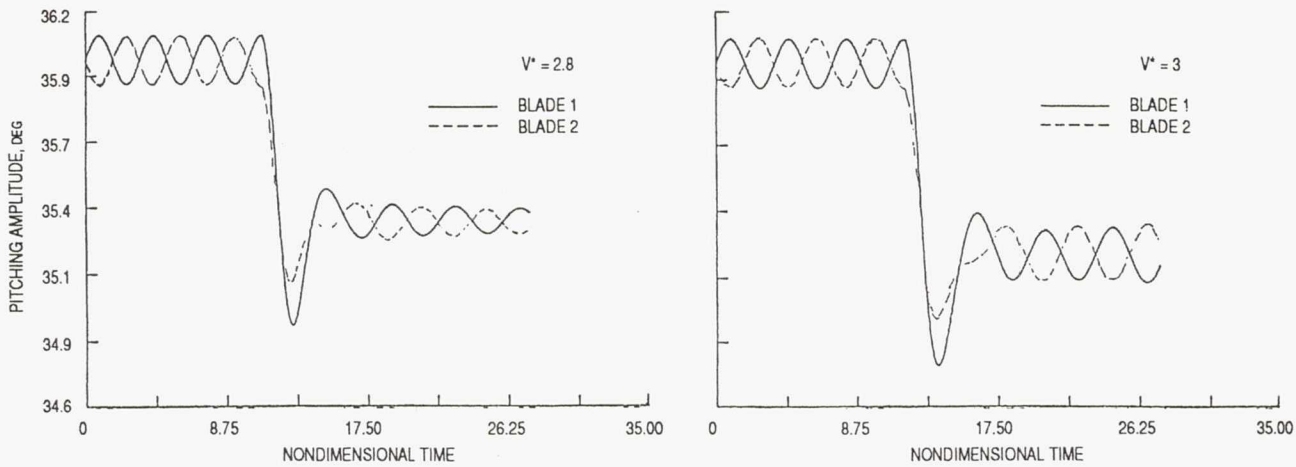

Figure 10.—Response of rotor section airfoil (parameters same as for Fig. 9; interblade phase angle σ = 180°; blades 1 and 2).

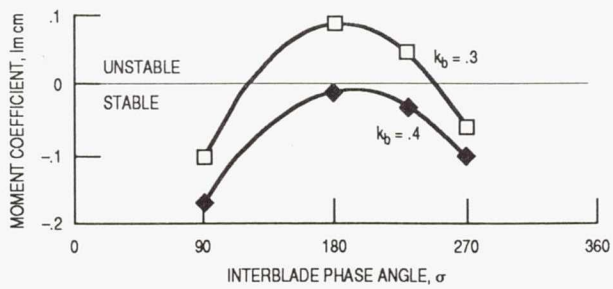

Figure 11.—Imaginary part of moment coefficient versus interblade phase angle (stator section airfoil; inlet Mach number M_1 = 2.72; stagger angle θ = 11.7°; inlet flow angle β = 23.3°; gap-to-chord ratio g/c = 0.297; pitching displacement α = 0.1 sin (ωt).

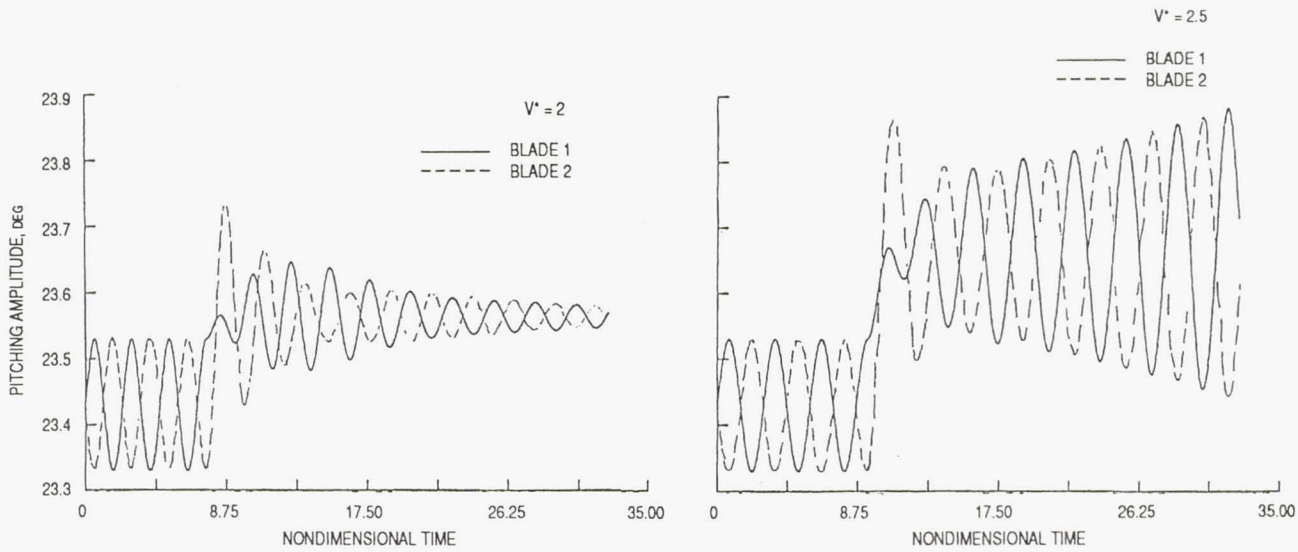

Figure 12.—Response of rotor section airfoil (parameters same as for Fig. 11; interblade phase angle $\sigma = 180°$; blades 1 and 2).

REPORT DOCUMENTATION PAGE

Form Approved
OMB No. 0704-0188

1. AGENCY USE ONLY (*Leave blank*)	2. REPORT DATE	3. REPORT TYPE AND DATES COVERED
	April 1992	Technical Memorandum

4. TITLE AND SUBTITLE

Flutter Analysis of a Supersonic Cascade in Time Domain Using an ADI Euler Solver

5. FUNDING NUMBERS

WU–535–03–01

6. AUTHOR(S)

T.S.R. Reddy, M.A. Bakhle, and D.L. Huff

7. PERFORMING ORGANIZATION NAME(S) AND ADDRESS(ES)

National Aeronautics and Space Administration
Lewis Research Center
Cleveland, Ohio 44135–3191

8. PERFORMING ORGANIZATION REPORT NUMBER

E–6966

9. SPONSORING/MONITORING AGENCY NAMES(S) AND ADDRESS(ES)

National Aeronautics and Space Administration
Washington, D.C. 20546–0001

10. SPONSORING/MONITORING AGENCY REPORT NUMBER

NASA TM–105625

11. SUPPLEMENTARY NOTES

T.S.R. Reddy and M.A. Bakhle, University of Toledo, Toledo, Ohio 43606 and NASA Resident Research Associate at Lewis Research Center. D.L. Huff, NASA Lewis Research Center. Responsible person, T.S.R. Reddy, (216) 433–6083.

12a. DISTRIBUTION/AVAILABILITY STATEMENT

LIMITED DISTRIBUTION DOCUMENT

Because of its significant technological potential, this information which has been developed under a U.S. Government program is being given a limited distribution whereby advanced access is provided for use by domestic interests. This legend shall be marked on any reproduction of this information in whole or in part.
Date for general release April 1994

Subject Category 39

12b. DISTRIBUTION CODE

13. ABSTRACT ***(Maximum 200 words)***

The aeroelastic stability of a two-dimensional cascade oscillating in supersonic axial flow is analyzed in the time domain. The aeroelastic model consists of a single-degree-of-freedom typical section structural model for each blade of the cascade and an unsteady two-dimensional cascade aerodynamic model based on the Euler equations. The Euler equations are solved using a time-accurate Alternating Direction Implicit (ADI) solution scheme. The aeroelastic equations are integrated in time. The effect of interblade phase angle is included in the aeroelastic analysis by an appropriate choice of initial and boundary conditions. Flutter predictions are obtained from the time response of a flat plate cascade in single-degree-of-freedom pitching motion. The results correlate well with those obtained from a separate frequency domain flutter analysis for all values of interblade phase angles considered. Flutter results are then presented for cascades having airfoil sections representative of a supersonic throughflow fan. The validity of the time integration method for a cascade of airfoils at various interblade phase angles is demonstrated.

14. SUBJECT TERMS	15. NUMBER OF PAGES
Cascades; Supersonic axial flow; Flutter; Frequency domain; Time domain	24
	16. PRICE CODE A03

17. SECURITY CLASSIFICATION OF REPORT	18. SECURITY CLASSIFICATION OF THIS PAGE	19. SECURITY CLASSIFICATION OF ABSTRACT	20. LIMITATION OF ABSTRACT
Unclassified	Unclassified	Unclassified	

National Aeronautics and
Space Administration

Lewis Research Center
Cleveland, Ohio 44135

FOURTH CLASS MAIL

ADDRESS CORRECTION REQUESTED

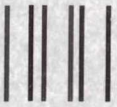

Postage and Fees Paid
National Aeronautics and
Space Administration
NASA 451

Official Business
Penalty for Private Use $300

NASA